Synsint Research Group

Available online at www.synsint.com

Synthesis and Sintering

ISSN 2564-0186 (Print), **ISSN** 2564-0194 (Online)

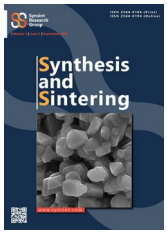

Research article

Enhancing the antibacterial properties of zinc sulfide thin films by substrate patterning

Fatemeh Abdi *, Solmaz Kia

Department of Engineering Sciences, Faculty of Advanced Technologies, University of Mohaghegh Ardabili, Namin, Iran

ABSTRACT

To investigate the porosity and substrate effects on the antibacterial properties of ZnS thin films, sculptured structures were considered. Two types of uncoated glass and primary coated glass were used as different substrates. Since the porosity percentage is dependent on the shadow of grains, spiral structures with different numbers of pitches were formed on the different substrates. The cross-section and morphology of the samples were investigated by means of FESEM images. To evaluate the antibacterial properties of the samples under light irradiation, the absorption spectra of the structures at different wavelengths were obtained and investigated. The results showed that most adsorption of structures occurs at wavelengths less than 400 nm. Finally, antibacterial properties of this thin film were investigated in two cases of without light and with light irradiation, for two types of Escherichia coli and Staphylococcus aureus bacteria. The results showed that the structures with higher porosity have better antibacterial properties. The results also showed that light radiation increases the antibacterial properties of structures.

KEYWORDS

Sculptured thin films
Spiral
Antibacterial property
Ultraviolet light
Zinc sulfide

OPEN ACCESS

1. Introduction

Semiconductors composed of group II-VI or III-V elements are good candidates for electrical, optical, and optoelectronic applications due to their wide energy gaps. At the nanoscale, the properties of materials are highly dependent on the shape and size of nanoparticles. Therefore, the fabrication of semiconductor nanostructures with various shapes and sizes and the investigation of their properties are of great interest [1–3]. ZnS (zinc sulfide) is one of the most popular semiconductors in group II-VI, which has two different cubic and hexagonal structures. In bulk dimensions, the energy gap of these two structures is 3.68 eV and 3.91 electron volts, respectively [1–4]. ZnS is a transparent material in the visible and infrared region, so it is a good candidate for optoelectronic devices such as emitting diodes [5–6] and solar cells [7–9]. It also has a wide range of applications in laser environments [10] and photocatalysts [11–14].

The dependence of the different properties on the dimensions has led to the formation of zinc sulfide thin films by various chemical and physical methods [15–20]. So far, the dependence of optical [21–26] and electrical [27–31] properties of this material on nanoparticle size has been extensively studied.

Oblique angle deposition and glancing angle deposition are two methods of forming nanostructures with different shapes and sizes. In the oblique deposition method, the evaporating flux lands on the substrate at oblique angles, so columnar structures are formed. In the glancing angle deposition method, the evaporating flux lands on the moving substrate. In this method, the shape of the structures is controlled by the substrate rotation around different axes [32]. In these methods, the primary atoms form shadow areas behind them, which are protected from the landing of other atoms [33, 34]. The shadow effect causes the descending atoms to join the primary nuclease and continue to grow in these regions [35–37]. Because of

* Corresponding author. *E-mail address:* F.Abdi@uma.ac.ir (F. Abdi)

Received 3 September 2025; Received in revised form 29 September 2025; Accepted 30 September 2025.

https://doi.org/10.53063/synsint.2025.53312

this shadowing effect, these structures are not uniform and are porous structures, and the degree of porosity is controlled by the angle of the incident flux. Sculptured thin films are columnar structures whose direction changes during the growth process. In these methods, the size of the structures can be controlled by controlling the initial nucleation [38–39]. The properties of these thin films are strongly dependent on the porosity percentage. For example, it has been shown that increasing porosity increases photocatalytic properties [40].

Today, structures based on various compounds of zinc and magnesium are very popular. These compounds can be used in medical fields such as tissue grafting, implants, bone repair, and surface coating due to their properties such as biocompatibility, biodegradability, ability to absorb high energy per unit mass, high specific resistance, and antibacterial properties [41–43]. The antibacterial properties of zinc sulfide nanoparticles have already been confirmed by various researchers [44, 45]. We showed in previous work that helical zinc sulfide thin film has antibacterial properties, and that the antibacterial properties increase with increasing number of helical turns. This work aims to increase the antibacterial properties by patterning the substrate. Using the glancing angle deposition method, ZnS spiral structures, with different numbers of pitches, were formed on different substrates, and their antibacterial properties and dependence on porosity were investigated.

Zinc sulfide (ZnS), a wide bandgap (3.6–3.9 eV) II-VI semiconductor, has emerged as a promising material for self-cleaning and sterilizing surfaces due to its intrinsic dual functionality: photocatalytic activity and antibacterial properties. When fabricated as thin films, these characteristics are often enhanced and become critical for applications in environmental remediation, water purification, and biomedical coatings. The fundamental link between the two properties lies in the photocatalytic process, which, upon UV or near-UV light irradiation, generates highly reactive species responsible for both pollutant degradation and microbial inactivation.

1- Photoexcitation: When a photon with energy equal to or greater than the ZnS bandgap (hν≥Eg) strikes the thin film, an electron (e^-) is promoted from the valence band (VB) to the conduction band (CB), creating a positive hole (h^+) in the VB:

$$ZnS + h\nu \rightarrow e^-_{CB} + h^+_{VB} \quad (1)$$

2- Reactive oxygen species (ROS) generation: The photogenerated charge carriers migrate to the surface of the ZnS film and react with adsorbed water and oxygen, leading to the formation of potent ROS:

- Hydroxyl radical (•OH): The hole (h^+) reacts with water molecules (H_2O) or hydroxyl ions (OH^-):

$$h^+_{VB} + H_2O \rightarrow \bullet OH + H^+ \quad (2)$$

$$h^+_{VB} + OH^- \rightarrow \bullet OH \quad (3)$$

- Superoxide radical anion ($\bullet O^{2-}$): The electron (e^-) reacts with molecular oxygen (O_2):

$$e^-_{CB} + O_2 \rightarrow \bullet O^{2-} \quad (4)$$

The ROS generated through the photocatalytic process are the primary agents of microbial destruction, establishing a direct link between the two phenomena [46–48].

The highly energetic and non-specific ROS (primarily •OH and $\bullet O^{2-}$) attack and compromise the fundamental components of bacterial cells, leading to inactivation or death.

- Cell membrane damage: The ROS attack the polyunsaturated fatty acids in the bacterial lipid cell membrane, causing lipid peroxidation. This increases the membrane's permeability, disrupts its structural integrity, and ultimately leads to cell leakage and lysis (rupture).
- Internal component disruption: The radicals penetrate the cell and oxidize essential intracellular components, including DNA, proteins, and enzymes, which are critical for respiration and replication, thereby halting all biological functions.

While less prominent in the overall antibacterial mechanism compared to ROS generation, the release of zinc ions (Zn^{2+}) from the ZnS surface can also contribute to the antibacterial effect. These ions can enter the bacterial cell and interfere with enzyme function and metabolic processes. The photocatalytic enhancement primarily stems from the ROS pathway, especially under illumination. The efficacy of the dual functionality in ZnS is highly dependent on the thin film's physical and electronic structure.

- Nanostructuring and morphology: Thin films composed of nanoparticles or nanorods exhibit an increased surface area-to-volume ratio, providing more active sites for light absorption and surface reactions, thereby accelerating the photocatalytic ROS production and improving contact with bacterial cells.
- Recombination inhibition: The efficiency is often limited by the rapid recombination of the photogenerated e^-/h^+ pairs. Strategies like metal doping (e.g., Ag, Cu, Mn) or forming heterojunctions (e.g., ZnO@ZnS) are employed to create internal electric fields that separate the charge carriers, prolonging their lifespan and significantly boosting ROS production and, consequently, the antibacterial activity [46–49].

2. Experimental

To investigate the effect of porosity on antibacterial properties, spiral thin films with different porosities were considered. Due to the fact that the substrate is effective in determining the initial nucleation for growth, spiral structures were formed on different substrates. One of the substrates was considered a smooth glass substrate with the least roughness, and the other substrate was considered a substrate with an initial core. To prepare this substrate with primary nucleation, the glasses were first cut to the dimensions of 1 mm ×20 mm ×20 mm and then cleaned in acetone and alcohol in an ultrasonic bath. A thin film of ZnS with a thickness of 7 nm was deposited on the glass substrate and heated to 350 °C. For the deposition of this ZnS thin film, we utilized an Edwards (Edwards E19 A3) system. ZnS with a purity of 99% was deposited by electron beam at room temperature and a base pressure of 2×10^{-7} mbar. By doing this, nanometer islands with an average diameter of 30 nm were formed, which were used as the initial nuclei for the growth of ZnS spiral nanostructures. Fig. 1 shows the islands formed on the glass due to heat. These ZnS thin films on glass and glass were considered as substrates for the growth of spiral structures.

To prepare the spiral structures, the substrates were glued to substrate holder using carbon double-sided adhesive (for vacuum). Electron beam evaporation was used for deposition Evaporation rate, deposition angle, (respect to perpendicular to the substrate) and

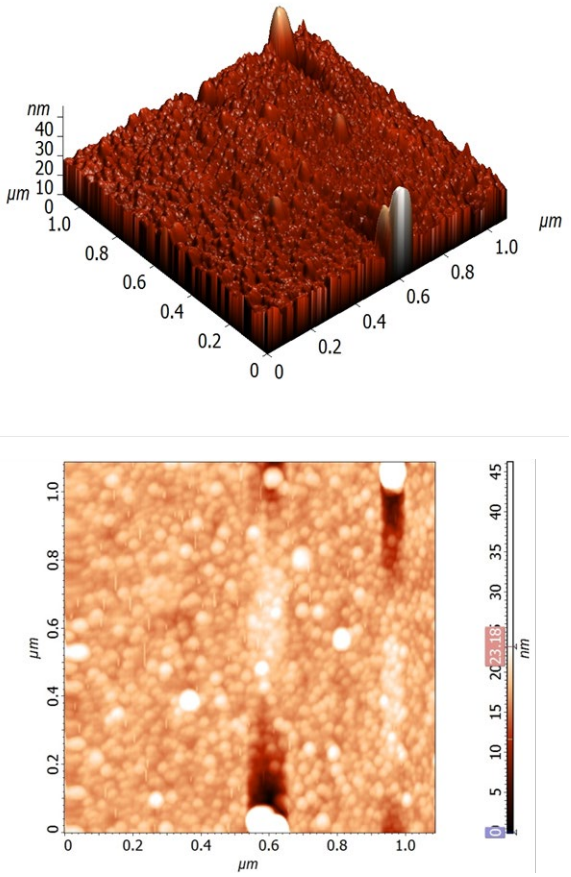

Fig. 1. Surface morphology of Zns/glass substrate-initial nucleation as seeds for second deposition.

rotation speed of the substrate was considered 1 Å/S, 75 ° and 0.04 rpm, respectively. In all the deposition time, the deposition rate and thickness of the spiral-thin films were monitored by the crystal quartz inspector. The initial pressure was 1.5×10^{-7} torr and the deposition was performed at room temperature. The rotating system was programmed to rotate one, three, and five turns of the substrate to construct spiral structures with a number of 1, 3 and 5 pitches. For the sake of brevity, the spiral structure on glass with one pitch, three pitches and five pitches were named G1, G3 and G5, respectively, and the spiral structures with one to 5 pitches on the substrate with the initial core were named ZG1, ZG3 and ZG5, respectively.

In this work, FESEM (Hitachi S-4800) was used to observe the surface and cross-section of spiral structures. For absorbance amount analysis of samples, the optical spectra of the samples were obtained using a single-beam spectrophotometer for p-polarized light at 10 ° incident light angle in the spectral range of 350–1000 nm.

2.1. Antibacterial testing

To investigate the antibacterial properties of Müller Hinton agar and D-glucose, it was purchased from Sigma Aldrich. Also, autoclave devices (Iran, Reyhan Teb Co., Model 2 RT-) and Memert incubator (Germany, Model 601BVM) were used to perform the work.

Finally, the dependence of antibacterial properties on the porosity of structures was investigated with and without light irradiation.

Escherichia coli (ATCC 8739) and Staphylococcus aureus (ATCC 6538) were selected as two infective bacterial strains and purchased from the Persian Type Culture Collection Center (Iran, Tehran). The bacterial strains were plated onto MHA and incubated at 37 °C/18–24 h, then some isolated colonies were transferred to an isotonic 0.264 M D-glucose solution, and turbidity was adjusted to 0.5 of the McFarland scale. Therefore, for the determination of cell viability, final bacterial cell concentrations in the suspensions were around 10^8 CFU/ml. To prevent inactivation of cationic sites by the high ionic strength or negatively charged molecules such as polysaccharides and amino acids, the 0.264 M D-glucose solution was used instead of any culture medium.

One hundred microliters of the bacterial suspension were dropped onto the coated surfaces, and the samples were incubated at 37 °C for 1 h. Thereafter, these 100 microliters were transferred to 10 ml of 0.264 M D-glucose isotonic solution in Falcon tubes and strongly vortexed. After that, their 1:100 and 1:10,000 dilutions were prepared subsequently. 0.1 ml aliquots of the final dilutions were withdrawn and plated on MHA plates. The plates were incubated at 37 °C for 24 h, and the CFU for each plate was read. These readings were converted into CFU/ml and log (CFU/ml). Controls were bare glass coverslips.

3. Results and discussion

3.1. FESEM results

Figs. 2 & 3 show the spiral structures formed on glass and 'ZnS on glass' substrates, respectively. It is clear from the figures that the spiral thin films formed on ZnS/glass substrate have larger grains than the other and have a higher porosity percentage. The reason for the larger grains formed on ZnS/glass is the presence of early places for growth. Because with the initial locations for growth, the surface diffusion length of the descending atoms decreases, and the grains grow preferentially at predetermined locations. In the substrates that do not have the initial nucleation, the grains begin to grow in the desired locations, and the primary grains are randomly placed in all possible parts of the substrate. For the substrate with initial nucleation, the shadow effect prevents growth in some areas, and this causes the films to become porous. The reason for the high porosity of the spiral thin films formed on the ZnS/glass substrate is the larger grain size and longer shadow length. It is clear from the images that as the number of pitches increases, the porosity of the thin films increases, which is due to the increase in shadow with increasing thickness. It is also clear from the FESEM images that the grain size increases with increasing number of pitches. The thickness, average grain size, and surface porosity percentage of different samples are given in Table 1. The results show that the one-pitch, three-pitch, and five-pitch structures have thicknesses of 80 nm, 240 nm, and 450 nm, respectively. The results also show that the surface porosity of the samples, which was obtained by subtracting the grain area from the total area, is higher for the structures formed on thin films than for the structures formed on glass. The porosity of the thin films on glass with one pitch, three pitches, and five pitches is 10%, 21%, and 25%, respectively, while the porosity of the similar structures on thin films is 15%, 27% and 31%, respectively. These results show that porosity increases with increasing thickness. The data in the table also show that structures formed on thin film have larger grains than structures formed on glass, due to the greater shadow effect, and the porosity of these structures is greater than similar structures on glass.

Table 1. Porosity percentage and average grain size of different structures.

Sample	Porosity percentage (%)	Thickness (nm)	Average grain size (nm)
G1	10	80	64
G3	21	240	90
G5	25	450	104
ZG1	15	80	78
ZG3	27	240	98
ZG5	31	450	124

3.2. Optical results

Photocatalytic properties are one of the attractive properties of semiconductors. Photovoltaic materials absorb photons and generate electron-hole pairs. This electron-hole pairs can react with molecules on the surface of particles and create a wide range of applications. One of these attractive applications is the use in antibacterial applications. To study the antibacterial properties of a semiconductor under light, its interaction with photons must be investigated.

Because zinc sulfide has photocatalytic properties, the absorption spectra (A) of samples were obtained using the optical spectrum (A=1-(R+T)). In this relation, R is a reflectance and T is a transmittance. These results are shown for spiral structures on the glass substrate in Fig. 4a and for similar structures on the ZnS/glass substrate in Fig. 4b.

The results show that structures with one pitch have little absorption in the visible spectrum and have only one absorption edge in the wavelength range less than 400 nm (ultraviolet region), which indicates the energy gap of the structures. As the number of pitches increases, the absorption in the visible range of the structures increases. These absorptions are related to interband transitions. The results show that the maximum absorption for all structures is at wavelengths less than 400 nm (ultraviolet region).

Using Eq. 5, the light absorption coefficient (α), which shows the photocatalytic ability of the material, was calculated for all structures. The results for structures formed on glass and ZnS/glass substrates are shown in Fig. 5a and Fig. 5b, respectively.

$$\alpha=2.303\times A/d \quad (5)$$

In the above relation, A is the absorption, and d is the thickness of the thin films. The results show that with increasing the number of pitches, the absorption coefficient increases. As the light absorption coefficient increases, the photocatalytic property increases. The results also show that the absorption edge for structures formed on ZnS/glass is shifted

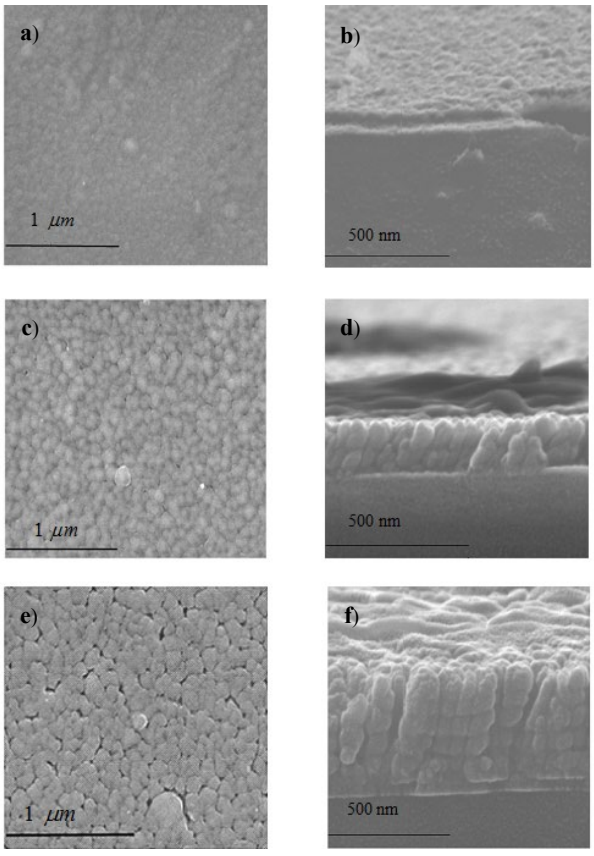

Fig. 2. FESEM images of ZnS spiral structures: a, b) G1, c, d) G3, and e, f) G5.

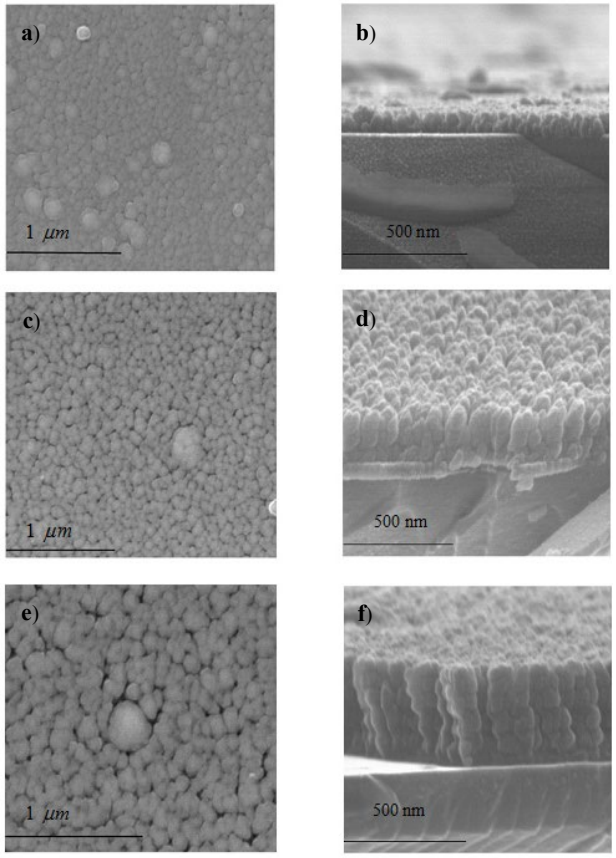

Fig. 3. FESEM images of ZnS spiral structures: a, b) ZG1, c, d) ZG3, and e, f) ZG5.

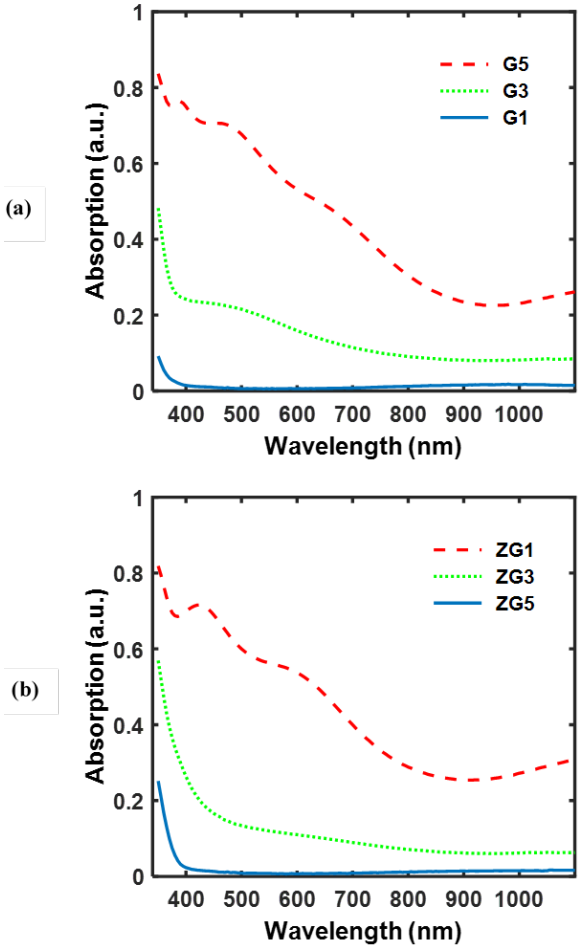

Fig. 4. Absorption spectra of ZnS spiral structures on: a) glass substrate and b) ZnS/glass substrate.

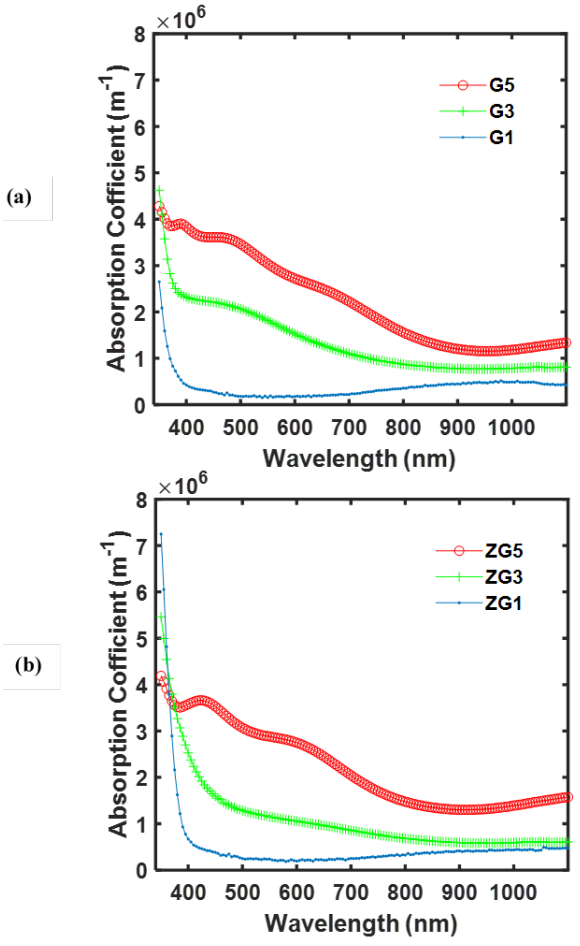

Fig. 5. Absorption coefficient of ZnS spiral structures on: a) glass substrate and b) ZnS/glass substrate.

towards long wavelengths. The reason for this displacement is the large grains of these structures, and as a result, the relative shrinkage of the energy gap of these structures compared to similar structures formed on the glass substrate. Due to the fact that the high absorption coefficient is related to wavelengths shorter than 400 nm, light with wavelengths shorter than 400 nm should be used to investigate the antibacterial properties under light irradiation.

3.3. Anti-bacterial results

These works were performed for the control sample and all spiral structures with different numbers of pitches formed on the glass and ZnS/glass substrates in two modes of without light irradiation and under light irradiation. The results of the measurements are reported in Table 2 and Fig. 6. Figs. 6a & 6b show the killing efficiency of different samples for Escherichia coli and Staphylococcus aureus bacteria in the absence of light, respectively.

It is clear from the figures that structures formed on ZnS/glass substrate have better antibacterial properties for both types of bacteria than similar structures grown on glass substrate. This is because of the higher porosity of these structures than those grown on glass, because with increasing porosity, the cross-sectional area of contact with bacteria increases. The results also show that due to the increase in porosity with increasing the number of pitches, the antibacterial property increases with increasing the number of pitches. These results show that structures with 5 pitches on the ZnS/glass substrate, due to the highest porosity percentage, have the highest bactericidal properties among all samples. These results are in agreement with our previous work [50].

To investigate the photocatalytic properties and their effect on the antibacterial properties of the samples, another experiment was performed under light irradiation. Because, according to the optical results, the maximum absorption of the structures occurred at wavelengths less than 400 nm, and the absorption edge was in the range of 300 nm to 400 nm, the experiment was performed under UVA light (315 to 400 nm) for all different structures. The results are given in the last column of Table 2 and the second row of Fig. 6. Figs. 6c & 6d show the killing efficiency of different samples for Escherichia coli and Staphylococcus aureus bacteria under light irradiation, respectively. These results show that UVA radiation enhances the antibacterial property. The reason for the increase in antibacterial properties under light radiation is the photocatalytic properties of

Table 2. Antibacterial activity of different structures.

Sample	Microorganism	Initial cell viability/log (CFU/ml)	Final cell viability/log (CFU/ml)	Final cell viability/log (CFU/ml) after radiation with UV light	Killing efficiency (C%)	Killing efficiency (C%) after radiation with UV light for 1 hour
Blank	E. coli	8.3	1.2	1.1	0	0
	S. aureus	8.2	1.1	1	0	0
G1	E. coli	8.3	1	0.9	5	15
	S. aureus	8.1	0.9	0.8	11	20
G3	E. coli	7.8	0.8	0.7	40	52
	S. aureus	8.2	0.7	0.6	46	57
G5	E. coli	8.3	0.5	0.4	61	75
	S. aureus	8.1	0.5	0.3	68	81

structures. In fact, under the light, the electron-hole pairs destroy the bacteria. In other words, in the presence of ultraviolet light, by supplying a gap energy, electrons kill bacteria by creating free radicals. The higher the light absorption, the more electrons produced and the better the antibacterial properties.

Optical results showed that with increasing the number of pitches, the absorption coefficient increases and as a result, the antibacterial property increases. The cell viability of S. aureus in the presence of control, G1, G3, and G5 samples under radiation was shown in Fig. 7a–d, respectively. Fig. 8a–d show these results for similar structures on ZnS/glass substrates. Therefore, spiral structures with 5 pitches on the ZnS/glass, under light radiation, because of the highest porosity percentage, have the best antibacterial properties among the other samples.

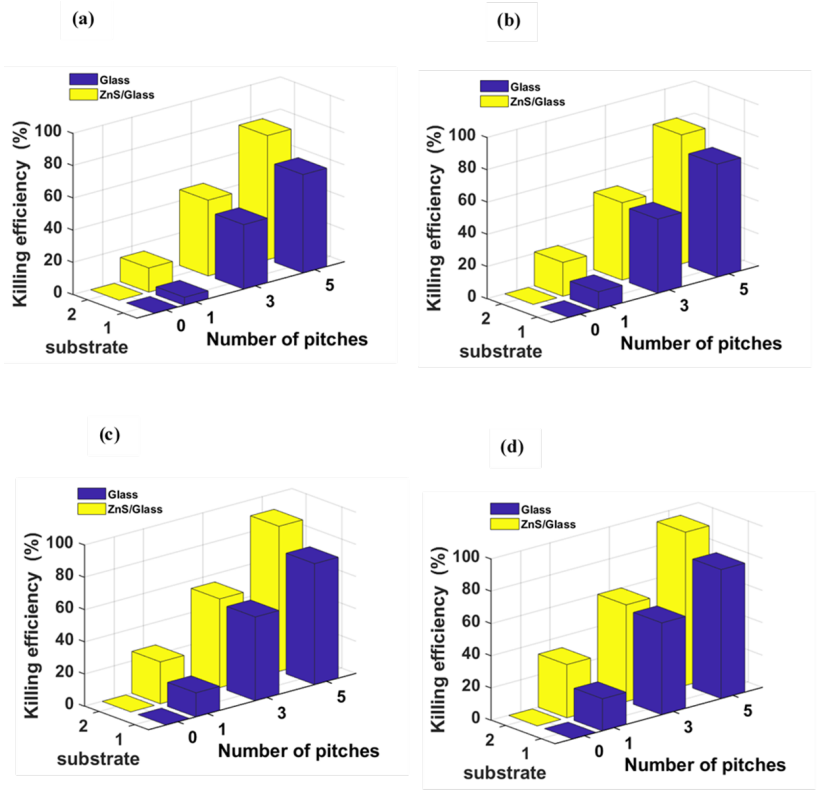

Fig. 6. Killing efficiency of ZnS spiral structures for: a) E. coli bacteria without light irradiation, b) S. aureus bacteria without radiation, c) E. coli bacteria with light irradiation, and d) S. aureus bacteria with radiation.

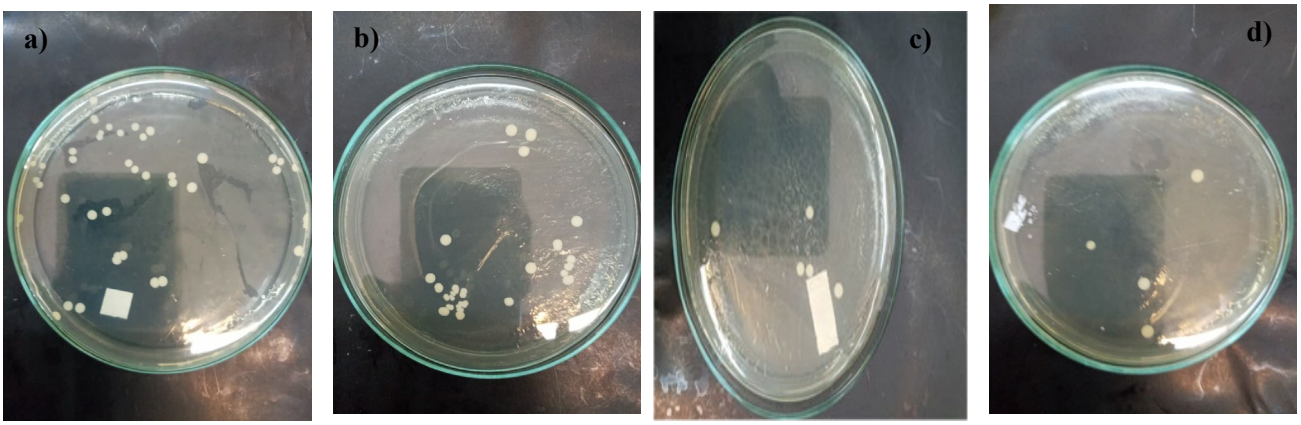

Fig. 7. Cell viability of S. aureus in the presence of: a) control sample, b) G1, c) G3, and d) G5.

4. Conclusions

In this work, to investigate the effect of substrate on the porosity and antibacterial properties of thin films, zinc sulfide spiral-shaped thin films with different numbers of pitches were formed on two types of glass substrates with primary nucleation and without primary nucleation. To prepare these structures, the glancing angle method was used. Morphology and cross-section of structures were investigated by means of FESEM images. FESEM images showed that with increasing the number of pitches due to the increase of the shadowing effect, the porosity of the structures increases. The results also showed that for the structures formed on the substrate with primary nucleation, due to the longer shadow length, the porosity of the structures is more than the other. The antibacterial properties of the structures were investigated for both types of Escherichia coli and Staphylococcus aureus bacteria, and the results showed that the antibacterial properties improve with increasing the number of pitches. The results also showed that the structures formed on the substrate with primary nucleation have better antibacterial properties than similar structures on glass. The reason was attributed to the increase in the porosity with the number of pitches, as well as the greater relative porosity of the structures grown on the substrate with the initial core than the similar structures on the glass, because with increasing porosity, the cross-sectional area of contact with bacteria increases. Given that sulfide is a semiconductor and has photocatalytic properties, to study the antibacterial properties under light, the absorption spectrum of the structures was obtained, and the absorption coefficient of the structures was calculated. Because the maximum absorption occurred at wavelengths less than 400 nm, the antibacterial properties under UVA light (315 nm to 400 nm) irradiation were investigated. The results showed that the spiral shape structure with 5 pitches on the ZnS/glass substrate with the highest porosity under light irradiation has the highest antibacterial properties and is the best candidate for antibacterial properties.

CRediT authorship contribution statement

Fatemeh Abdi: Conceptualization, Data curation, Formal Analysis, Investigation, Methodology, Project administration, Resources, Software, Supervision, Writing – original draft, Writing – review & editing.
Solmaz Kia: Writing – review & editing, Investigation.

Data availability

The data underlying this article will be shared on reasonable request to the corresponding author.

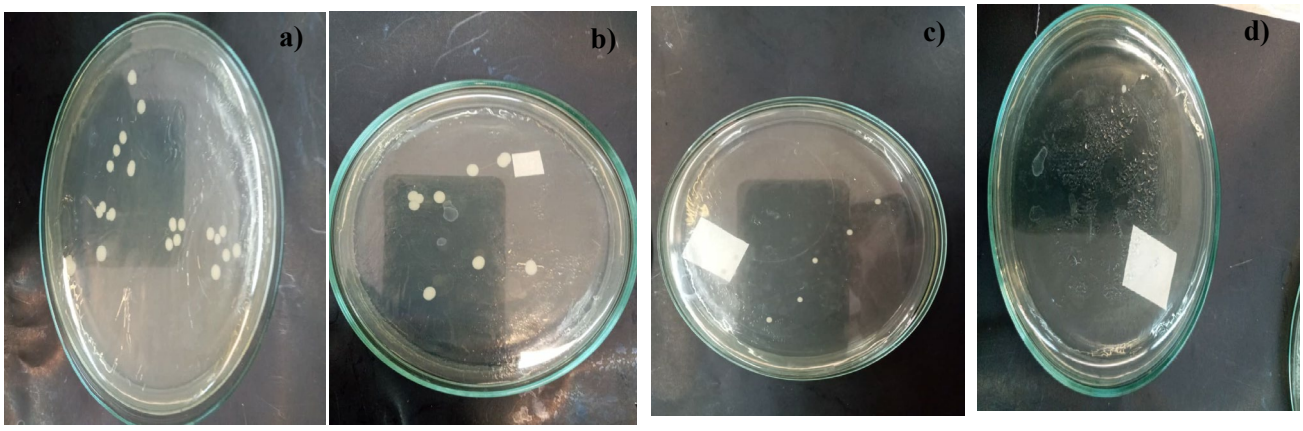

Fig. 8. Cell viability of S. aureus in the presence of: a) control sample, b) ZG1, c) ZG3, and d) ZG5.

Declaration of competing interest

The authors declare no competing interests.

Funding and acknowledgment

We would like to thank the University of Tehran and University of Mohaghegh Ardabili for their support.

References

[1] W.C. Chan, D.J. Maxwell, X. Gao, R.E. Bailey, M. Han, S. Nie, Luminescent quantum dots for multiplexed biological detection and imaging, Curr. Opin. Biotechnol. 13 (2002) 40–46. https://doi.org/10.1016/S0958-1669(02)00282-3.

[2] L. Coultas, K. Chawengsaksophak, J. Rossant, Endothelial cells and VEGF in vascular development, Nature. 438 (2005) 937–945. https://doi.org/10.1038/nature04479.

[3] W.C. Chan, S. Nie, Quantum dot bioconjugates for ultrasensitive nonisotopic detection, Science. 281 (1998) 2016–2018. https://doi.org/10.1126/science.281.5385.2016.

[4] G.R. Amiri, M.H. Yousefi, M.R. Aboulhassani, M.H. Keshavarz, D. Shahbazi, et al., Radar absorption of Ni0.7Zn0.3Fe2O4 nanoparticles, Digest J. Nanomater. Biostruct. 5 (2010) 719–725.

[5] W.H. Yang, G.C. Schatz, R.P. Duyne, Discrete dipole approximation for calculating extinction and Raman intensities for small particles with arbitrary shapes, J. Chem. Phys. 103 (1995) 869–875. https://doi.org/10.1063/1.469787.

[6] H. Katayama, S. Oda, H. Kukimoto, ZnS blue-light-emitting diodes with an external quantum efficiency of 5× 10−4, Appl. Phys. Lett. 27 (1975) 697–699. https://doi.org/10.1063/1.88350.

[7] N. Fathy, R. Kobayashi, M. Ichimura, Preparation of ZnS thin films by the pulsed electrochemical deposition, Mater. Sci. Eng: B. 107 (2004) 271–276. https://doi.org/10.1016/j.mseb.2003.11.021.

[8] A. Ates, M.A. Yıldırım, M. Kundakcı, A. Astam, Annealing and light effect on optical and electrical properties of ZnS thin films grown with the Silar method, Mater. Sci. Semicond. Process. 10 (2007) 281–286. https://doi.org/10.1016/j.mssp.2008.04.003.

[9] D. Lincot, R.O. Borges, Chemical bath deposition of cadmium sulfide thin films. In situ growth and structural studies by combined quartz crystal microbalance and electrochemical impedance techniques, J. Electrochem. Soc. 139 (1992) 1880. https://doi.org/10.1149/1.2069515.

[10] T.V. Prevenslik, Acoustoluminescence and sonoluminescence, J. Lumin. 87 (2000) 1210–1212. https://doi.org/10.1016/S0022-2313(99)00513-X.

[11] D. Chen, F. Huang, G. Ren, D. Li, M. Zheng, et al., ZnS nano-architectures: photocatalysis, deactivation and regeneration, Nanoscale. 2 (2010) 2062–2064. https://doi.org/10.1039/C0NR00171F.

[12] S. Yanagida, K. Mizumoto, C. Pac, Semiconductor photocatalysis. Part 6. Cis-trans photoisomerization of simple alkenes induced by trapped holes at surface states, J. Am. Chem. Soc. 108 (1986) 647–654. https://doi.org/10.1021/ja00264a014.

[13] J.S. Hu, L.L. Ren, Y.G. Guo, H.P. Liang, A.M. Cao, et al., Mass production and high photocatalytic activity of ZnS nanoporous nanoparticles, Angew. Chem. 117 (2005) 1295–1299. https://doi.org/10.1002/anie.200462057.

[14] H. Fujiwara, K. Murakoshi, Y. Wada, S. Yanagida, Observation of adsorbed N, N-dimethylformamide molecules on colloidal ZnS nanocrystallites, Effect of coexistent counteranion on surface structure, Langmuir. 14 (1998) 4070–4073. https://doi.org/10.1021/la9712855.

[15] M.P. Valkonen, S. Lindroos, T. Kanniainen, M. Leskelä, U. Tapper, E. Kauppinen, Thin multilayer CdS/ZnS films grown by Silar technique, Appl. Surf. Sci. 120 (1997) 58–64. https://doi.org/10.1016/S0169-4332(97)00248-1.

[16] Y.F. Nicolau, J.C. Menard, Solution growth of ZnS, CdS and Zn1-xCdxS thin films by the successive ionic-layer adsorption and reaction process; growth mechanism, J. Cryst. growth. 92 (1988) 128–142. https://doi.org/10.1016/0022-0248(88)90443-5.

[17] H. Murray, A. Tosser, Photoconduction et effets photovoltaïques dans des couches minces pulverisées de ZnS, Thin Solid Films. 24 (1974) 165–180. https://doi.org/10.1016/0040-6090(74)90262-4.

[18] H.L. Kwok, A study of ultra-thin CuxS-CdyZn1-yS polycrystalline solar cells, J. Phys. D: Appl. Phys. 16 (1983) 2367. https://doi.org/10.1088/0022-3727/16/12/015.

[19] O.M. Hussain, P.S. Reddy, B.S. Naidu, S. Uthanna, P.J. Reddy, Characterization of thin film ZnCdS/CdTe solar cell, Semicond. Sci. Technol. 6 (1991) 690. https://doi.org/10.1088/0268-1242/6/7/023.

[20] J.M. Doña, J. Herrero, Process and film characterization of chemical-bath-deposited ZnS thin films, J. Electrochem. Soc. 141 (1994) 205. https://doi.org/10.1149/1.2054685.

[21] F. Rahman, M. Zahan, J. Podder, Synthesis of nanocrystalline ZnS thin films via spray pyrolysis for optoelectronic devices, Sens. Transduc. 149 (2013) 54–59.

[22] J. Lee, S. Lee, S. Cho, S. Kim, L.Y. Park, Y.D. Choi, Role of growth parameters on structural and optical properties of ZnS nanocluster thin films grown by solution growth technique, Mater. Chem. Phys. 77 (2003) 254–260. https://doi.org/10.1016/S0254-0584(01)00563-6.

[23] I. Dékány, L. Nagy, L.Turi, Z. Király, N.A. Kotov, J.H. Fendler, Preparation and characterization of CdS and ZnS particles in nanophase reactors provided by binary liquids adsorbed at colloidal silica particles, Langmuir. 12 (1996) 3709–3715. https://doi.org/10.1021/la951541i.

[24] P.K. Ghosh, S. Jana, S. Nandy, K.K. Chattopadhyay, Size-dependent optical and dielectric properties of nanocrystalline ZnS thin films synthesized via rf-magnetron sputtering technique, Mater. Res. Bull. 42 (2007) 505–514. https://doi.org/10.1016/j.materresbull.2006.06.019.

[25] M.Y. Nadeem, W. Ahmed, Optical properties of ZnS thin films, Turk. J. Phys. 24 (2000) 651–659.

[26] H.J. Lee, S.I. Lee, Deposition and optical properties of nanocrystalline ZnS thin films by a chemical method, Curr. Appl. Phys. 7 (2007) 193–197. https://doi.org/10.1016/j.cap.2006.03.005.

[27] T. Asahi, H. Yamashita, T. Maekawa, Preparation and optical properties of ZnS-microcrystals deposited in silica gels, Ceram. Int. 27 (2001) 39–43. https://doi.org/10.1016/S0272-8842(00)00039-0.

[28] N. Fathy, M. Ichimura, Photoelectrical properties of ZnS thin films deposited from aqueous solution using pulsed electrochemical deposition, Sol. Energy Mater. 87 (2005) 747–756. https://doi.org/10.1016/j.solmat.2004.07.048.

[29] M.A. Yildirim, A. Ateş, A. Astam, Annealing and light effect on structural, optical and electrical properties of CuS, CuZnS and ZnS thin films grown by the silar method, Phys. E: Low-dimens. Sys. Nanostruct. 41 (2009) 1365–1372. https://doi.org/10.1016/j.physe.2009.04.014.

[30] H.K. Sadekar, N.G. Deshpande, Y.G. Gudage, A. Ghosh, S.D. Chavhan, et al., Growth, structural, optical and electrical study of ZnS thin films deposited by solution growth technique (SGT), J. Alloys Compd. 453 (2008) 519–524. https://doi.org/10.1016/j.jallcom.2007.10.123.

[31] B. Elidrissi, M. Addou, M. Regragui, A. Bougrine, A. Kachouane, J.C. Bernede, Structure, composition and optical properties of ZnS thin films prepared by spray pyrolysis, Mater. Chem. Phys. 68 (2001) 175–179. https://doi.org/10.1016/S0254-0584(00)00351-5.

[32] H.F. Zhang, C.M. Wang, E.C. Buck, L.S. Wang, Synthesis, characterization, and manipulation of helical SiO2 nanosprings, Nano Lett. 3 (2003) 577–580. https://doi.org/10.1021/nl0341180.

[33] F. Wang, A. Lakhtakia, Response of slanted chiral sculptured thin films to dipolar sources, Opt. Commun. 235 (2004) 133–151. https://doi.org/10.1016/j.optcom.2004.03.016.

[34] F. Wang, A. Lakhtakia, Lateral shifts of optical beams on reflection by slanted chiral sculptured thin films, Opt. Commun. 235 (2004) 107–132. https://doi.org/10.1016/j.optcom.2004.02.050.
[35] J.M. Nieuwenhuizen, H.B. Haanstra, Microfractography of thin films, Philips Tech. Rev. 27 (1966) 87–91.
[36] R. Messier, J.E. Yehoda, Geometry of thin-film morphology, J. Appl. Phys. 58 (1985) 3739–3746. https://doi.org/10.1063/1.335639.
[37] T. Motohiro,Y. Taga, Thin film retardation plate by oblique deposition, Appl. Opt. 28 (1989) 2466–2482. https://doi.org/10.1364/AO.28.002466.
[38] K. Robbie, M.J. Brett, Sculptured thin films and glancing angle deposition: Growth mechanics and applications, J. Vac. Sci. Technol. A: Vac. Surf. Films. 15 (1997) 1460–1465. https://doi.org/10.1116/1.580562.
[39] S.R. Kennedy, M.J. Brett, O. Toader, S. John, Fabrication of tetragonal square spiral photonic crystals, Nano Lett. 2 (2002) 59–62. https://doi.org/10.1021/nl015635q.
[40] W. Daranfed, M.S. Aida, A. Hafdallah, H. Lekiket, Substrate temperature influence on ZnS thin films prepared by ultrasonic spray, Thin Solid Films. 518 (2009) 1082–1084. https://doi.org/10.1016/j.tsf.2009.03.227.
[41] P.K. Bowen, J. Drelich, J. Goldman, Zinc exhibits ideal physiological corrosion behavior for bioabsorbable stents, Adv. Mater. 25 (2013) 2577–2582. https://doi.org/10.1002/adma.201300226.
[42] D. Vojtěch, J. Kubásek, J. Šerák, P. Novák, Mechanical and corrosion properties of newly developed biodegradable Zn-based alloys for bone fixation, Acta Biomater. 7 (2011) 3515–3522. https://doi.org/10.1016/j.actbio.2011.05.008.
[43] A.D. Campo, C. Echeverría, M.S. Martín, R.C. Rodríguez, M.F. García, A.M. Bonilla, Porous Microstructured Surfaces with pH-Triggered Antibacterial Properties, Macromol. Biosci. 19 (2019) 1900127. https://doi.org/10.1002/mabi.201900127.
[44] Z. Morshedtalab, G. Rahimi, A. Emami-Nejad, A. Farasat, A. Mohammadbeygi, et al., Antibacterial assessment of zinc sulfide nanoparticles against Streptococcus pyogenes and Acinetobacter baumannii, Curr. Top. Med. Chem. 20 (2020) 1042–1055. https://doi.org/10.2174/1381612826666200406095246.
[45] G.R. Amir, S. Fatahian, N. Kianpour, Investigation of ZnS nanoparticle antibacterial effect, Curr. Nanosci. 10 (2014) 796–800. https://doi.org/10.2174/15734137106661406042200007.
[46] S.K. Mani, M. Saroja, M. Venkatachalam, T. Rajamanickam, Antimicrobial activity and photocatalytic degradation properties of zinc sulfide nanoparticles synthesized by using plant extracts, J. Nanostruct. 8 (2018) 107–118. https://doi.org/10.22052/JNS.2018.02.001.
[47] F.W. Aldbea, Z. Abdoorhman, R.A. Almahdi, M. Kraini, N.A. Imrigha, Structural Properties and Antibacterial Activity of Zinc Sulfide Nanoparticles, NanoWorld J. 9 (2023) 127–132. https://doi.org/10.17756/nwj.2023-124.
[48] K.R. Raghupathi, R.T. Koodali, A.C. Manna, Size-dependent bacterial growth inhibition and mechanism of antibacterial activity of zinc oxide nanoparticles, Langmuir. 27 (2011) 4020–4028. https://doi.org/10.1021/la104825u.
[49] F. Long, W.M. Wang, Z.K. Cui, L.Z. Fan, Z.G. Zou, T.K. Jia, An improved method for chemical bath deposition of ZnS thin films, Chem. Phys. Lett. 462 (2008) 84–87. https://doi.org/10.1016/j.cplett.2008.07.064.
[50] F. Abdi, S. Kia, Designing and fabrication of zinc sulfide helical shape sculptured thin films and study of antibacterial properties of these porous structures, Metall. Eng. 24 (2021) 42–49. https://doi.org/10.22076/me.2022.527132.1312.